High Temperature Oxidation of Refractory High Entropy Alloys (RHEAs) and the Use of High Entropy Rare Earth Oxide (HERO) Coatings

Thesis

Presented in Partial Fulfillment of the Requirements for the Honors Research Distinction in the Undergraduate School of The Ohio State University

By

Isabella A. Marino

Undergraduate Program in Materials Science and Engineering

The Ohio State University

2024

Thesis Committee

Jenifer S. (Warner) Locke, Advisor

Stephen R. Niezgoda

Copyrighted by

Isabella A. Marino

2024

Abstract

Refractory high entropy alloys (RHEAs) possess favorable material properties, such as high melting points, resistance to corrosion, microstructural stability, and mechanical strength, which makes them a strong candidate for aerospace, automotive, and nuclear applications. To ensure safe high temperature performance, understanding and minimizing the rate of oxygen diffusion, and specifically high temperature oxidation, in RHEAs is imperative. The inherent high temperature oxidation performance of two RHEA compositions provided by the United States Air Force Research Laboratory are being investigated, after varying high temperature exposures in a controlled oxygen environment for various time intervals. Additionally, the effects of surrounding each alloy in a high entropy rare earth oxide (HERO) sintered powder sheath provided by the University of Virginia is investigated under identical conditions. Dilatometry is used to compare thermal expansion between the substrates and HERO coating. Thermogravimetric analysis is used to measure oxidation resistance and SEM and X-ray techniques are used to understand the microstructure.

Acknowledgments

The research reported here was sponsored by the Bob Rapp Visiting Scholar fund at The Ohio State University, which is in honor of Prof. Robert Rapp's long career in education and research. Davis S. Williams is the key, primary benefactor and creator of the Bobb Rapp visiting scholar fund at OSU. Significant benefactors include Dr. David S. Williams, Dr. Robert H. Wagoner, Dr. John P. Hirth, Dr. Robert Rapp, and Mr. William T. Weisert. These benefactors account for about 85% (over $200,000) raised for this fund.

The inaugural Bob Rapp Visiting Scholar position is currently held by Dr. Daniel B. Miracle, Senior Scientist in the Materials and Manufacturing Directorate of the Air Force Research Laboratory (AFRL). I would like to thank Dr. Miracle for his immense support throughout this project. His guidance, insights, and encouragement were invaluable. I would also like to thank Oleg N. Senkov (AFRL) for his key role in researching and designing the RHEA compositions presented in this study.

Dr. Beth J. Opila, leader of the Advanced High Temperature Materials research group at the University of Virginia, provided guidance and expertise in the areas of HERO coatings and high temperature oxidation kinetics. I would like to thank Dr. Opila and the University of Virginia for hosting me at the Opila laboratory for two weeks to conduct research for this project. I would also like to thank the following students from the University of Virginia that assisted me with experiment execution and data analysis done in this project: Charlie Brandenburg, Pádraigín Stack, Clark Luckhardt, Rachel Rosner, Sarah Beth Holles, and Catherine Lynch.

I owe a special thank-you to my advisor, Dr. Jenifer Locke, advisor at Ohio State's Fontana Corrosion Center. Dr. Locke has not only been an academic mentor to me for the past two years, but she has also been a personal role model. She has taught me about hard work, dedication, and believing in myself. Her passion for materials science and the encouragement she provides to her students is inspiring. The work done in this project would not have been possible without her support.

I would also like to thank a few people in the MSE department at The Ohio State University that have assisted me at various points throughout this project. Gabby Montiel has been an important mentor to me that has never failed to offer advice and materials science insights. Wayne Papageorge taught me how to prepare samples for metallographic analysis and provided invaluable tips about polishing. I would also like to thank Dr. Steve Niezgoda for being a member of my thesis defense committee and asking me challenging questions that encouraged me to think deeper.

Additionally, I would like to extend my gratitude to my sister, Gabriella Marino. Gabriella has inspired me through her passion of materials science and has encouraged me since a young age to embrace and pursue a future in STEM. She has been a constant role model in my life and has helped shape me into the person I am today.

Electron microscopy was performed at the Center for Electron Microscopy and Analysis (CEMAS) at The Ohio State University.

Table of Contents

List of Tables

List of Figures

Chapter 1. Introduction

1.1 Background and Motivation

High entropy alloys (HEAs) can be defined on a compositional basis as alloys with at least 5 principal elements, each having concentrations between 5 and 35 weight percent. These alloys can also include minor additions of various elements to alter their base properties [1]. HEAs are characterized by four core effects, which differentiate them from other materials. The first effect, known as the high entropy effect, implies that the increased configurational entropy in these alloys favor solid solution phases over typical intermetallic compounds [2]. The second, lattice distortion effect refers to the increased severity of lattice distortion and configurational entropy in HEAs due to the variation in atom sizes that compose the crystal lattice [2]. These distortions increase hardness, reduce electrical and thermal conductivity, and reduce the dependence these properties have on temperature [2]. The third, sluggish diffusion effect refers to slowed diffusion in HEAs due to the formation of nanocrystals and amorphous phases during the cooling process [2]. The fourth effect, referred to as the 'cocktail' effect, describes how unexpected, synergistic results can be the outcome of unusual combinations of materials and microstructures [2]. In addition to these favorable and unique effects specific to HEAs, they are also reported to possess good wear, fatigue, and corrosion resistance, as well as high temperature strength due to their high melting points [3].

Refractory elements, such as Nb, Cr, and Mo, are also known for their resistance to corrosion, wear, and high temperature degradation [4]. Conventional refractory alloys are commonly used in aerospace and other high temperature environment industries for their optimal performance at higher temperatures. However, at temperatures exceeding about 1200°C, conventional refractory alloys fail to perform well due to the formation of nonprotective oxides [4]. Oxidation in these alloys causes embrittlement and cracking, which leads to material degradation and opportunities for internal oxidation [4]. Volatile oxides may form in these locations further into the bulk of the substrate, causing an attack on the grain boundaries and disintegration of the metal into a powder form, which is a process known as pesting [4].

One solution to this problem has been to utilize refractory high entropy alloys (RHEAs) rather than conventional ones. RHEAs are HEAs with high concentrations of refractory elements. RHEAs are still subject to oxidation at high temperatures but have significantly improved oxidation rates due to their enhanced microstructural stability, sluggish diffusion, and ability to form protective oxide layers when oxidation does occur [4]. There have been three primary methods to protect RHEAs from oxygen diffusion: (1) adding concentrations Al, Cr, Si, and other elements to promote the production of protective oxide layers, (2) adding concentrations of other elements to promote the production of complex oxides that hinder oxygen diffusion, and (3) applying surface coatings to the RHEA to protect the substrate from the environment [4]. However, it is important to note that even well-performing protective oxide layers result in some level of internal oxidation and nitridation, and damage to mechanical properties at room temperature [5]. Furthermore, well-performing complex oxide layers demonstrate linear oxidation kinetics after a few hours at high temperatures, and even pesting at intermediate temperatures [4]. However, limited studies have been performed to demonstrate the effect of coatings on RHEAs [4].

Notable coatings that have been tested on conventional refractory alloys are high entropy rare earth oxide (HERO) coatings. Rare earth oxides have been proven to maintain stability at high temperatures with high velocity steam, as well as minimize oxygen diffusivity [6]. Researchers at the University of Virginia (UVa) have recently conducted studies to test the effect of HERO coatings on the oxidation kinetics of the C-103 alloy (Nb based alloy with Hf and Ti additions) [6]. They concluded that the HERO coating had excellent steam resistance, environmental contaminant resistance, and low thermal conductivity; however, internal oxidation of Hf was observed at increasing depths as a function of exposure time [6].

1.2 Research Objectives

This work is a result of the collaborative efforts of the Locke Lab within the Fontana Corrosion Center at OSU, the Opila Lab at UVa, and Dr. Dan Miracle's team at the Materials and Manufacturing Directorate at the AFRL. The overall research objective for this project is to understand and evaluate the oxidation of two compositions of RHEAs at high temperatures, as well as to evaluate the performance of each when surrounded by a HERO sintered powder bed. Specific objectives are listed below.

- Understand and characterize the microstructures of two RHEAs before high temperature exposure
- Quantify the amount of oxidation for two different RHEA compositions after high temperature exposure
- Understand the compatibility between the HERO powder bed and the RHEA

- Surround both RHEA compositions with the HERO sintered powder to understand if and how the HERO composition can protect the RHEA from oxidation

1.3 Thesis Overview

The research objectives are addressed throughout the different chapters in this Thesis. Chapter 2 focuses on the sample preparation for both RHEAs studied in this project, as well as the application method for the HERO sintered powder to the substrates. It also addresses the different methods used to characterize the RHEAs, such as dilatometry, thermogravimetric analysis (TGA), scanning electron microscopy (SEM), and X-ray techniques. Chapter 3 explores the results of these characterization techniques. SEM/EDS images and graphs support the microstructural analysis of both RHEAs. Dilatometry results are used to calculate and assess the coefficients of thermal expansion (CTE) of the alloys, as well as compare those values to published data of the CTE of the HERO sintered powder. The high temperature oxidation kinetics are quantified from the results of TGA, and X-ray diffraction (XRD) is used to characterize the oxide layers formed during this exposure. Lastly, Chapter 4 states the main conclusions drawn from these studies.

Chapter 2. Methodology

2.1 RHEA Sample Preparation

Two RHEAs were produced via arc melting of high purity elements, by and at the AFRL. Alloy 1-3 was fabricated with a composition of 70 Nb – 15 Mo – 9 Ti – 3 Hf – 3 W (at%), and Alloy 2-8 with a composition of 53 Nb – 25 Mo – 10 Ti – 9 Cr – 3 Si (at%). Ensuing arc melting, both alloys underwent hot isostatic press (HIP) in pure Argon at 1400°C and 30,000 psi for 3 hours. Individual test samples used in this study, including cylinders (5 mm diameter X 20 mm length), buttons (10 mm diameter X 3 mm thick), and coupons (3 mm length X 20 mm width X 2 mm thick), were cut from each bulk alloy via electrical discharge machining (EDM). Prior to any further testing, all samples were polished to 600 grit finish with silicon carbide. Polished samples were sonicated in de-ionized (DI) water, acetone, and/or ethanol.

2.2 HERO Application to RHEA

The utilization of a HERO sintered powder bed was examined as a potential environmental barrier to reduce the oxidation kinetics of Alloy 1-3 and Alloy 2-8 at high temperatures. The HERO sintered powder bed, which will be referred to as a "coating" throughout the rest of this document, surrounded buttons of both alloys via spark plasma sintering (SPS).

The composition of the HERO powder was $(Y_{0.33}Yb_{0.33}Er_{0.33})_2O_3$, courtesy of Oerlikon Metco. The powder was calcined at 600°C for 40 minutes before being ball milled for at least 18 hours with Zirconia sintering beads. Approximately 7.5 grams of HERO powder was used to coat each RHEA button. Initially, about 3.5 grams of HERO powder was input into the bottom half of a graphite die that was lined with graphite foil and plugged on the bottom with a graphite punch. After the first addition of the HERO powder, the RHEA button was placed in the center of the die. Subsequently, the remaining 4.0 grams of HERO powder was poured into the die and secured in place with another punch.

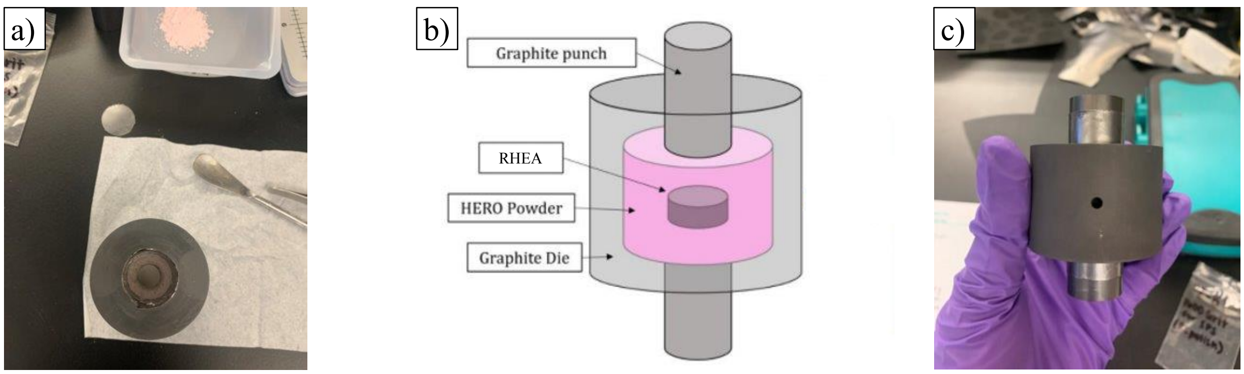

Figure 2.1: (a) Bird's eye view of the RHEA button placed on top of HERO powder inside of the graphite die used for SPS, (b) Schematic of the SPS processing system used to coat the RHEA button with sintered HERO powder [7], and (c) completed SPS processing system prior to entering the SPS chamber.

The graphite die, graphite punch, and RHEA complex was placed in an SPS chamber, where it reached a maximum pressure of 65 MPa and temperature of 1500°C for 10 minutes in pure Ar.

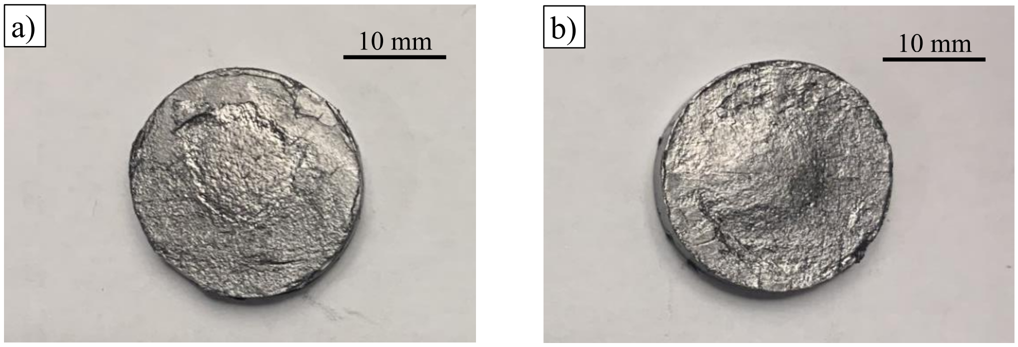

Figure 2.2: HERO powder sintered on RHEA substrate of (a) Alloy 2-8 and (b) Alloy 1-3.

2.3 RHEA Characterization

A scanning electron microscope (SEM), equipped with backscatter electron (BSE) and secondary electron (SE) imaging, was used to examine surface topographies and compositional differences in Alloys 1-3 and 2-8. RHEA buttons were polished to a 0.5 micron colloidal silica finish, and SEM images were taken with energy dispersive X-ray spectroscopy (EDS) analysis.

The coefficient of thermal expansion (CTE) of Alloys 1-3 and 2-8 were measured with a dilatometer. A standard alumina test was performed prior to tests on each alloy to calibrate the machine and provide a reference point for the results produced by the RHEA. Alumina tests were run in the dilatometer up to 1200°C in pure Argon for 2 hours. After each alumina test, Alloy 1-3 and Alloy 2-8 cylindrical samples were analyzed in the dilatometer under identical conditions.

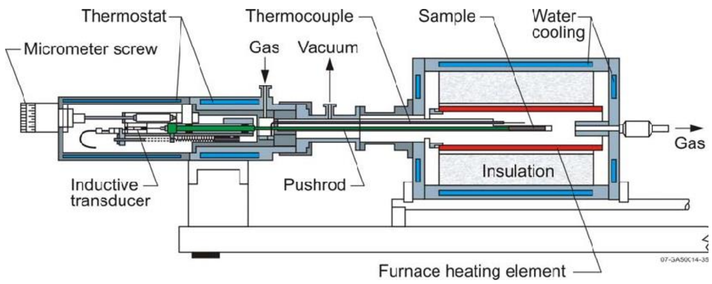

Figure 2.3: Schematic of a dilatometer, similar to the one used in this study [8].

Oxidation kinetics tests were performed via thermogravimetric analysis (TGA). Coated and non-coated RHEA buttons, as well as non-coated RHEA rectangular coupons, were hung in a TGA machine for 5.5 hours at an isothermal 1150°C in 1% O_2 in Ar, flowing at 100 cc/min. The oxide compositions formed on the non-coated RHEA rectangular coupons were analyzed with X-ray diffraction (XRD).

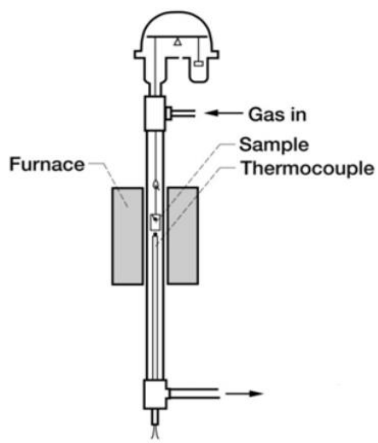

Figure 2.4: Schematic of a TGA machine, similar to the one used in this study.

Chapter 3. Results & Discussion

3.1 SEM Images

Baseline characterization of Alloys 1-3 and 2-8 were performed using a Thermo Scientific Apreo SEM to gather an initial analysis of the microstructures for both substrates prior to coating. To gain a better understanding of the surface conditions and topography of the RHEA substrates before applying the HERO coating, Alloy 2-8 was examined at the same 600 grit surface finish that existed prior to coating and TGA exposure.

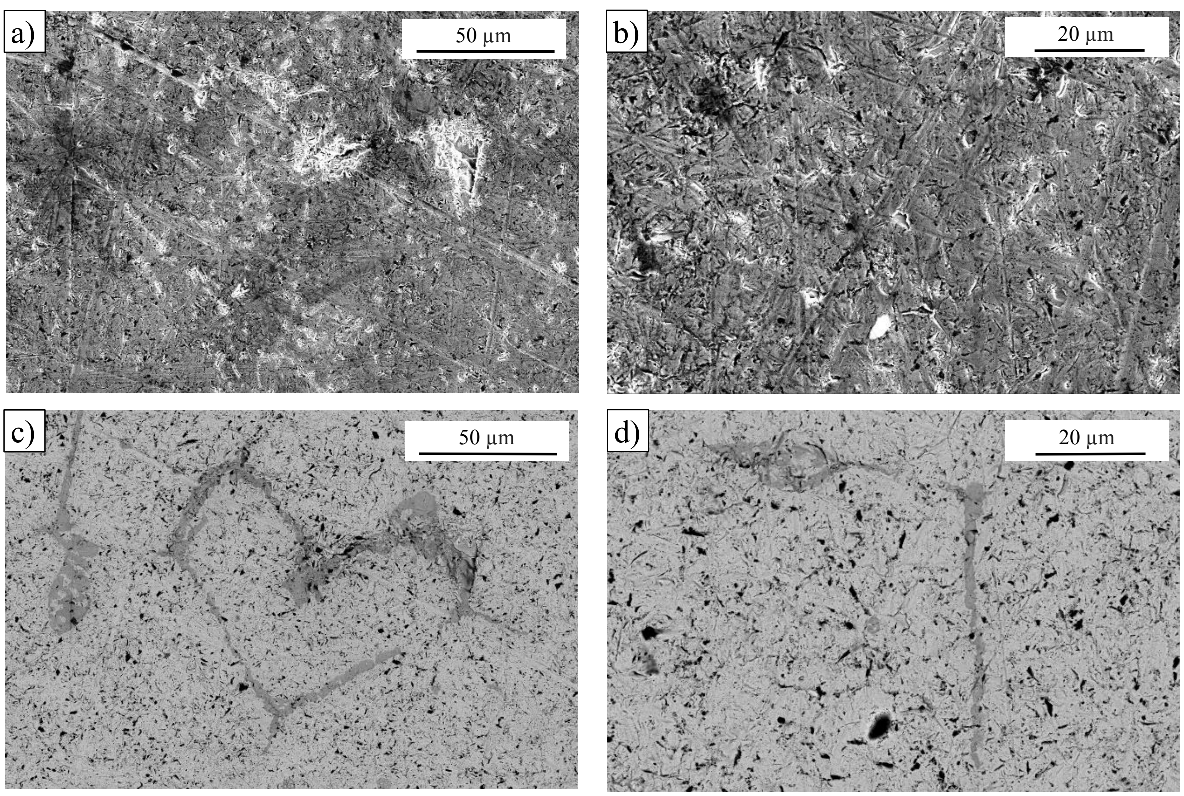

Figure 3.1: SEM images of Alloy 2-8 with a 600 grit surface finish at varying magnifications. (a) and (b) are taken with SE imaging, and (c) and (d) are taken via BSE imaging.

Figure 3.1 displays the SEM images taken of Alloy 2-8, using an accelerating voltage of 15.00 kV and beam current of 1.6 nA. Point EDS analysis was performed on the imaged section in Figure 3.1 (c).

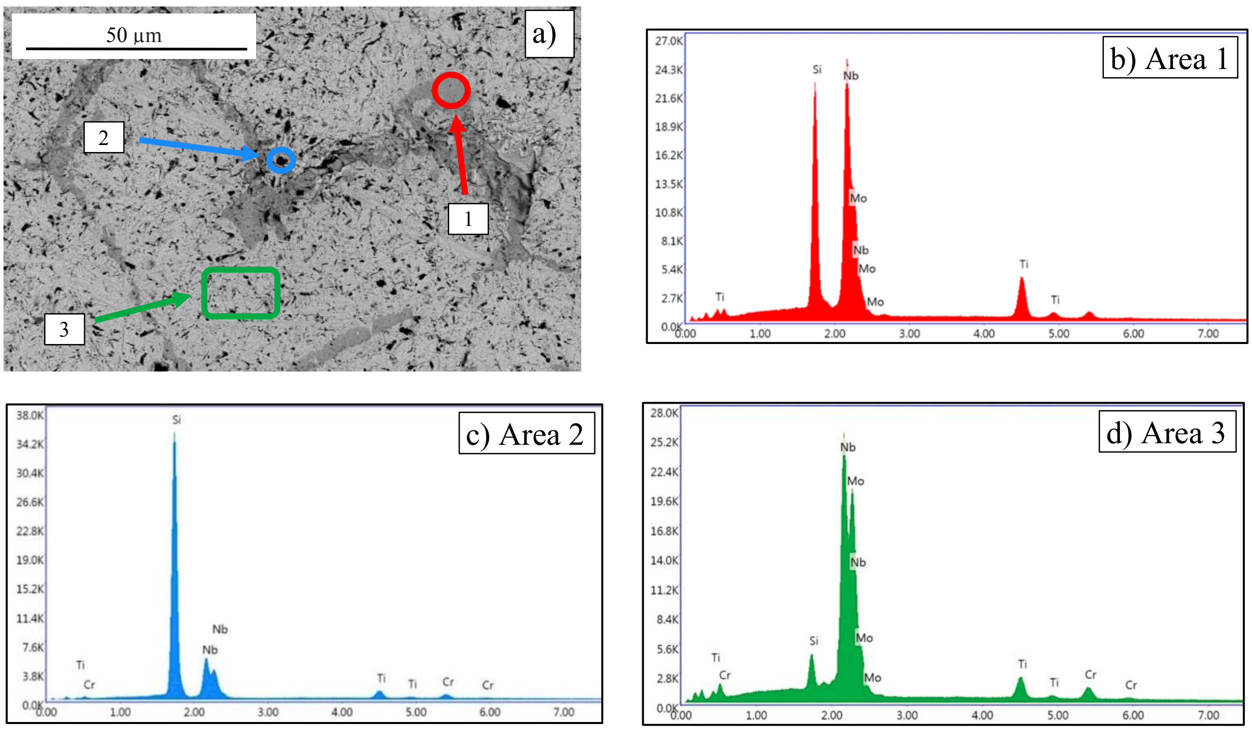

Figure 3.2: (a) BSE image taken of Alloy 2-8 at 600 grit surface finish with labeled areas that were analyzed with EDS, (b) EDS spectra of the lighter grey portion of Alloy 2-8, labeled Area 1, (c) EDS spectra of the darkest portion of Alloy 2-8, labeled Area 2, and (d) EDS spectra of the bulk material of Alloy 2-8, labeled Area 3.

Figure 3.2 illustrates that the bulk material (area 3 displayed in green) in Alloy 2-8 is primarily composed of a Nb – Mo rich phase, with trace amounts of Si, Ti, and Cr. The darker grey secondary phase (area 1 displayed in red) has a similar composition to the bulk, excluding a heavy concentration of Si and no traceable amounts of Cr. The darkest secondary phase particles (area 2 displayed in blue) are primarily Si with a small amount of Nb and trace amounts of Ti and Cr.

To collect more precise images, devoid of contamination from polishing or large scratches from rough surface finishes, Alloys 2-8 and 1-3 were polished to a 0.5 micron colloidal silica finish and examined under the SEM with EDS analysis.

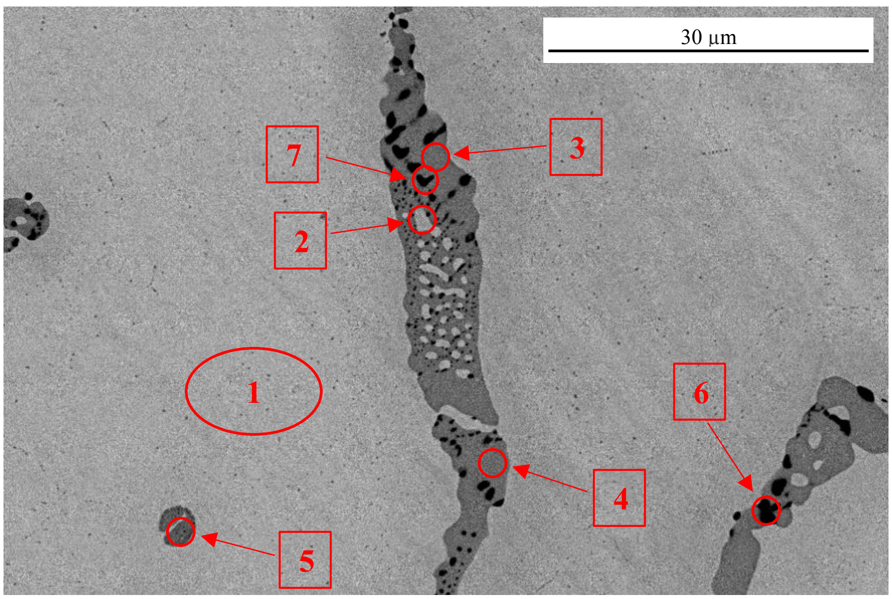

Figure 3.3: BSE image taken of Alloy 2-8 at 0.5 micron colloidal silica surface finish with labeled areas that were analyzed with EDS.

Figure 3.3 displays Alloy 2-8 at a higher magnification (2500 X) than shown in Figure 3.2 (1000 X), but at an identical accelerating voltage of 15.00 kV and beam current of 1.6 nA. The corresponding EDS spectra for each area labeled in Figure 3.3 can be found in Appendix A. The findings of this EDS analysis were comparable to the analysis performed with the 600 grit polish. The lighter grey phase of the bulk material (areas 1 and 2) is primarily Nb – Mo rich, with trace amounts of Ti and Cr. The darker grey secondary phases (areas 3, 4, and 5) are primarily Nb and Si with trace amounts of Ti. The black, submicron secondary phases (areas 6 and 7) are primarily Ti with small amounts of Nb. Although the other regions are nearly identical to the EDS results at 600 grit, the darker, smaller secondary phases showed to be primarily Si with trace amounts of Ti at the rougher surface finish, which is displayed in Figure 3.2 (c).

Alloy 1-3 was examined at an accelerating voltage of 10.00 kV and a beam current of 3.2 nA under the SEM with EDS analysis. The EDS spectra in Figure 3.4 (b) is representative of the bulk material in Alloy 1-3 shown in Figure 3.4 (a). These images show that Alloy 1-3 has large grains that contain small, submicron secondary phase particles.

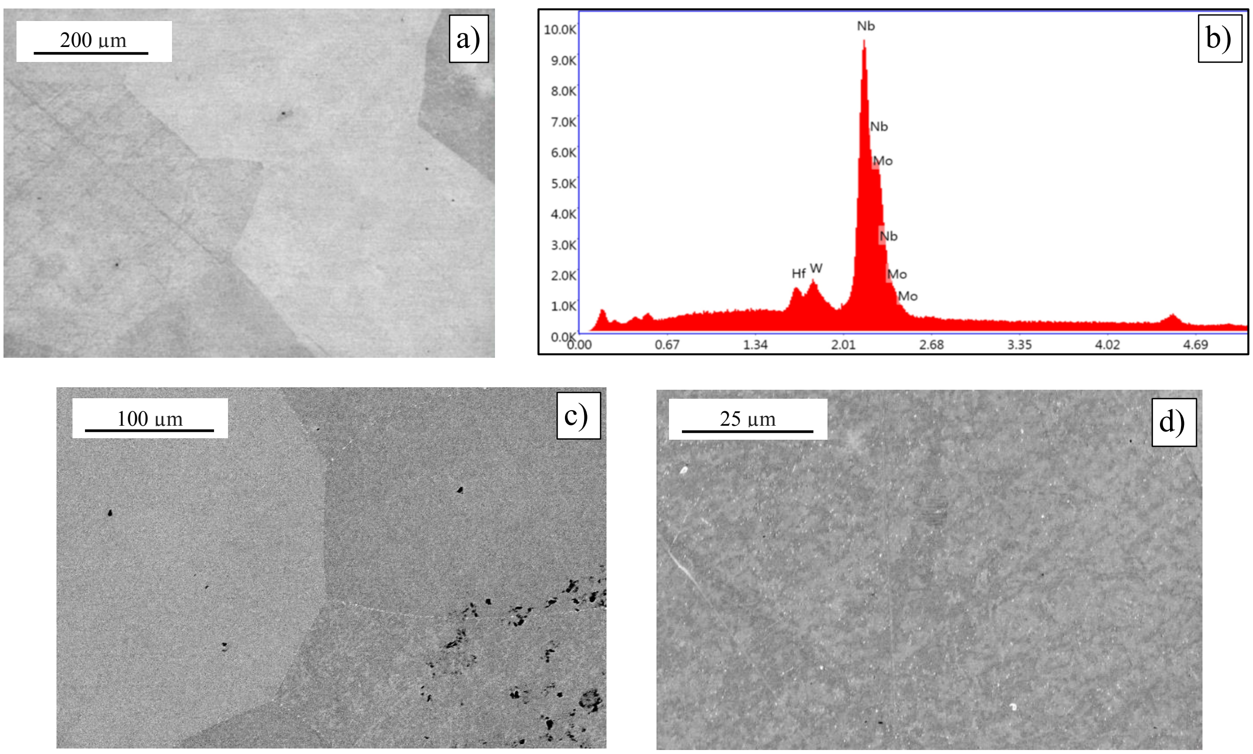

Figure 3.4: (a), (c), (d) BSE images taken of Alloy 2-8 at 0.5 micron colloidal silica surface finish; (b) EDS spectra of the bulk material of Alloy 1-3 taken from (a).

3.2 Dilatometry

Understanding the thermal expansion of the alloys studied in this project aids in understanding the oxidation kinetics of the substrates, as well as assessing the compatibility of the substrates with the HERO coating. A dilatometer was used to measure the CTE of Alloys 1-3 and 2-8.

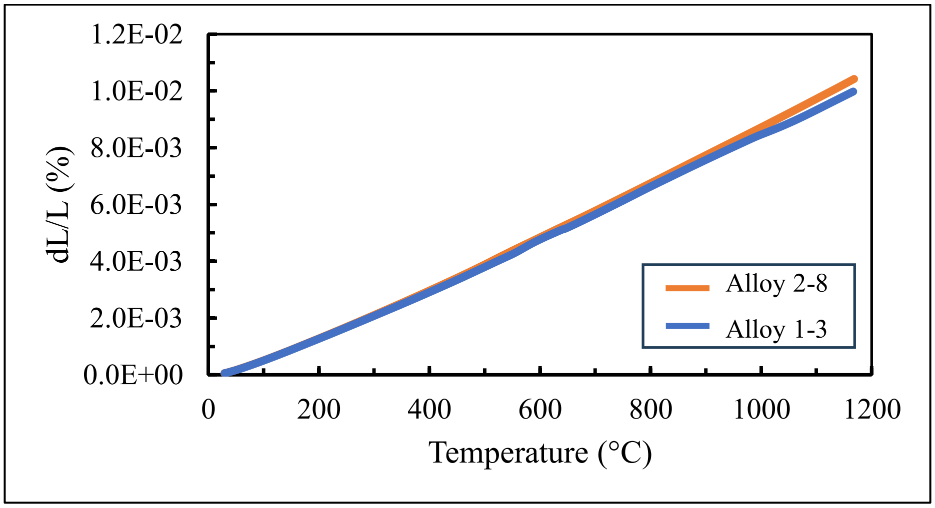

Figure 3.5: Graph illustrating the percent change in length with temperature of Alloys 1-3 and 2-8 over a 2-hour interval in pure Ar, reaching a maximum temperature of about 1200°C.

Figure 3.5 illustrates the expansion of the alloys with respect to their original lengths as a function of temperature. Both alloys have a strong linear correlation between their percent expansion with respect to temperature; however, it can be noted that Alloy 1-3 appears to slightly deviate from linearity at about 600°C and 1000°C. These results were used to calculate the average and instantaneous linear CTEs. Figure 3.6 compares the instantaneous CTE of both RHEAs and the $(Y,Yb,Er)_2O_3$ HERO coating being studied in this project. Alloy 1-3 has considerable disturbances in CTE at about 600°C and 1000°C. A potential reason for these disturbances can be explained by phase changes that occur in Alloy 1-3 at these temperatures. SEM analysis must be conducted in order to confirm if this phase change hypothesis holds.

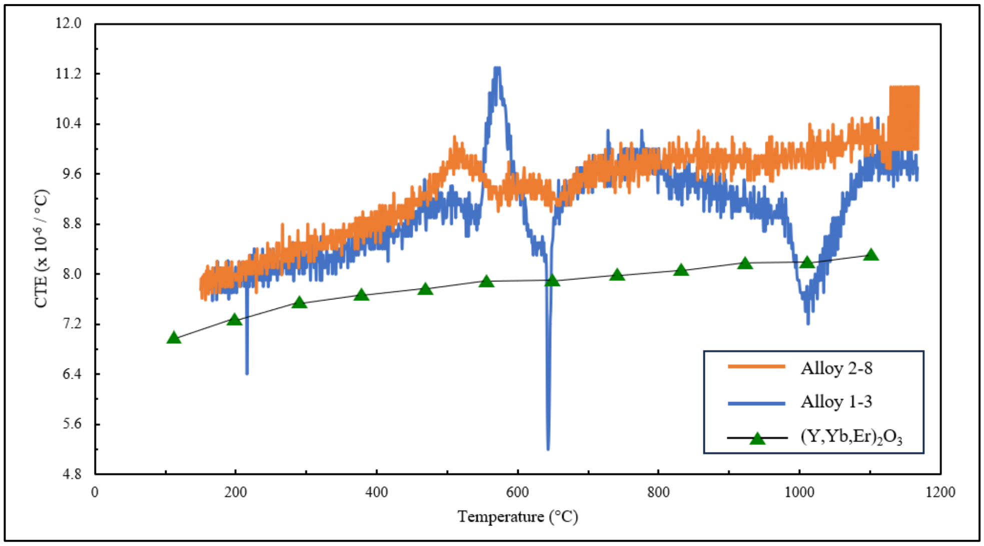

Figure 3.6: Graph illustrating the instantaneous coefficient of thermal expansion as a function of temperature of Alloy 1-3, Alloy 2-8, and the HERO coating examined in this study. Data for Alloys 1-3 and 2-8 was collected in a 2-hour interval in pure Ar, reaching a maximum temperature of about 1200°C. The CTE data for the HERO coating that is displayed was provided by the Opila Lab at the University of Virginia [6].

Alloys 2-8 and 1-3 have very similar CTEs and follow comparable trajectories with respect to an increase in temperature. The CTE of the HERO coating is smaller than the CTEs of both alloys, which is a potential concern for its utility. A mismatch of thermal expansion between the alloy substrate and HERO coating can lead to increased cracking and accelerated degradation. Cracking can occur when the substrate expands at a faster rate than the coating, which increases the stress the alloy endures and exposes it to the oxidizing environment. Table 1 highlights the average CTE values calculated for both alloys, as well as provides a range of values for the coating. The CTE of the HERO coating results were provided by the Opila research group at the University of Virginia [6].

Table 1: Average CTE values calculated for Alloys 2-8 and 1-3 for the 150°C – 1200°C temperature range based on the dilatometer data described in Figure 3.6. A range was given for the average CTE of the HERO coating instead of a single value, which was based on data provided by the Opila research group at the University of Virginia [6].

Material	CTE [150°C - 1200°C] ($x\ 10^{-6}$ / °C)
Alloy 2-8	9.37
Alloy 1-3	8.95
$(Y,Yb,Er)_2O_3$	6.8 - 8.0

3.3 Thermogravimetric Analysis

Uncoated Alloys

The oxidation kinetics of Alloys 2-8 and 1-3 were studied through thermogravimetric analysis (TGA). The mass gain with respect to each sample's surface area was plotted against time after undergoing 1150°C exposure in 1% O_2 in Ar in the TGA machine.

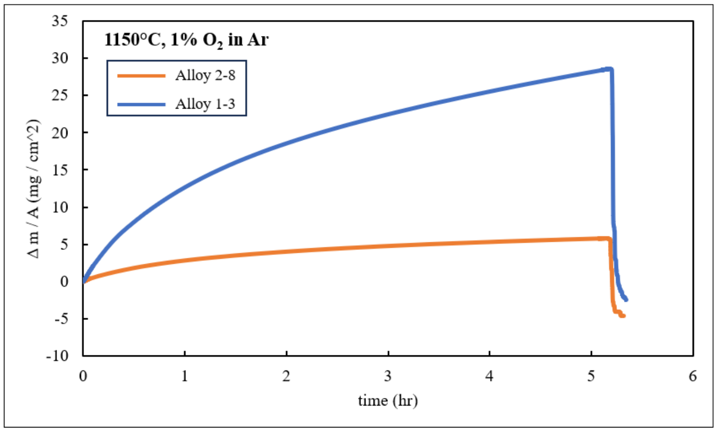

Figure 3.7: Graph illustrating the mass gain oxidation kinetics of rectangular shaped coupon samples of Alloys 1-3 and 2-8 after undergoing TGA exposure at 1150°C for 5.5 hours in 1% O_2 in Ar.

The results in Figure 3.7 indicate that both Alloys 2-8 and 1-3 demonstrate a parabolic diffusion rate of oxidation; however, Alloy 2-8 has a smaller, less damaging mass gain. The maximum $\Delta m/A$ observed in Alloy 2-8 was 5.85 mg/cm^2 and the maximum in Alloy 1-3 was 28.60 mg/cm^2. There is a considerable drop in mass of both alloys after about 5 hours of exposure, which was due to a spallation of oxide layers during cooling. The oxidation is apparent in the visual appearance of the sample coupons after being taken out of the TGA machine, which can be seen in Figure 3.8.

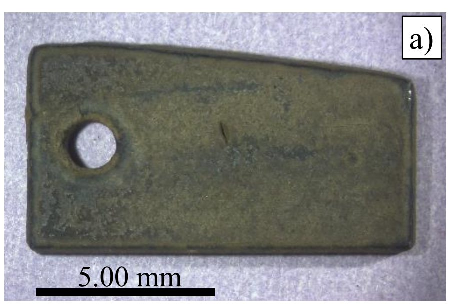

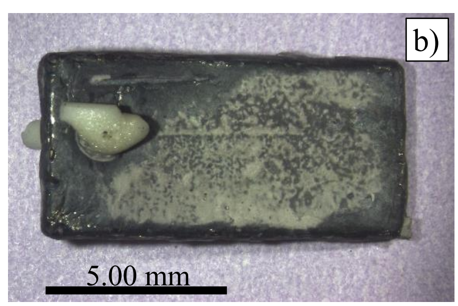

Figure 3.8: Images of rectangular shaped coupon samples after undergoing TGA conditions described in Figure 3.7 for (a) Alloy 2-8 and (b) Alloy 1-3. The cream colored fragment located in the hole of the coupon sample in (b) is the tip of the TGA hook, which was unable to come out after take-down of the experiment.

In order to confirm the repeatability of these results, these experiments were repeated again under the same conditions, but with different sample geometries; button shaped samples were used instead of the rectangular shaped samples seen above. The results of this experiment were analogous to the one done prior.

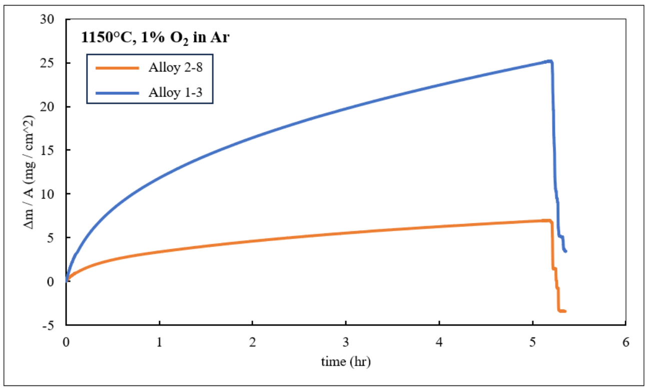

Figure 3.9: Graph illustrating the mass gain oxidation kinetics of button shaped samples of Alloys 1-3 and 2-8 after undergoing TGA exposure at 1150°C for 5.5 hours in 1% O_2 in Ar.

As shown in the previous TGA results, both alloys had parabolic oxidation kinetics, but Alloy 2-8 had a more sluggish diffusion rate as evidence by the lower mass gain. The mass gain with respect to surface area in this study was comparable to the study done on the rectangular coupon samples, as the maximum in this study was 6.98 mg/cm^2 for Alloy 2-8 and 25.23 mg/cm^2 in Alloy 1-3. The samples in both studies also have similar colored and textured surfaces, supporting that similar oxide layers formed during high temperature exposure in both trials. These images, in addition to images of the samples prior to oxidation, can be seen in Figure 3.10.

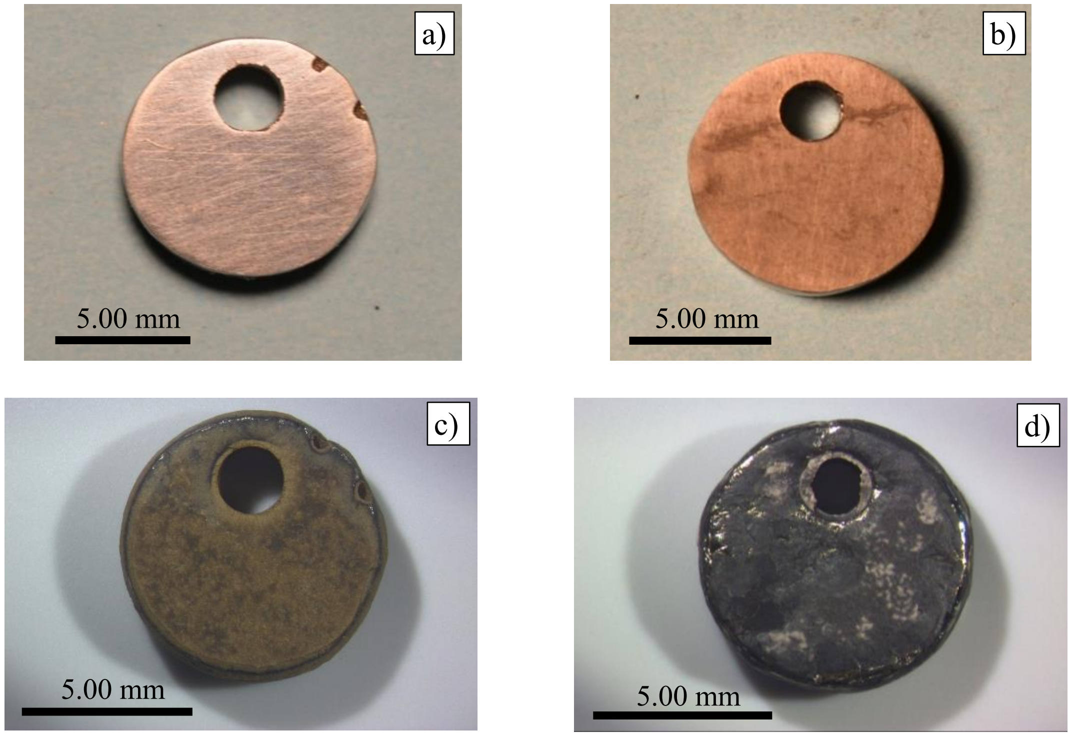

Figure 3.10: Images of button shaped coupon samples used in TGA experiments, as described in Figure 3.9. Images of buttons prior to high temperature exposure can be seen in (a) for Alloy 2-8 and (b) Alloy 1-3. Images of buttons after high temperature exposure can be seen in (c) for Alloy 2-8 and (d) Alloy 1-3.

Coated Alloys

HERO coated samples of Alloys 2-8 and 1-3 were also run in the TGA under identical conditions. These were hung with a platinum wire, as drilling a hole in them would compromise the integrity of the coating. The HERO coated sample of Alloy 2-8 had an initial diameter of 20.02 mm. The inner diameter of the tube used in the TGA machine is about 21.5 mm, which could have resulted in the sample hitting the inner walls of the tube during the duration of the experiment. The data collected in this study had insufficient quality for meaningful analysis of the oxidation kinetics, possibly due to the sample hitting the inner tube wall. For Alloy 1-3, the initial mass was 9.32 grams prior to TGA exposure, which is significantly higher than most sample masses that have been analyzed in the TGA machine and led to mechanical failures. The TGA wire connected to the balance broke and caused the sample to fall and get caught near the bottom of the furnace. This test also resulted in data that could not be used for meaningful analysis of the oxidation kinetics; however, the microstructures of the samples can be assessed in future work to examine the depth and formation of oxide layers that occurred in the TGA machine.

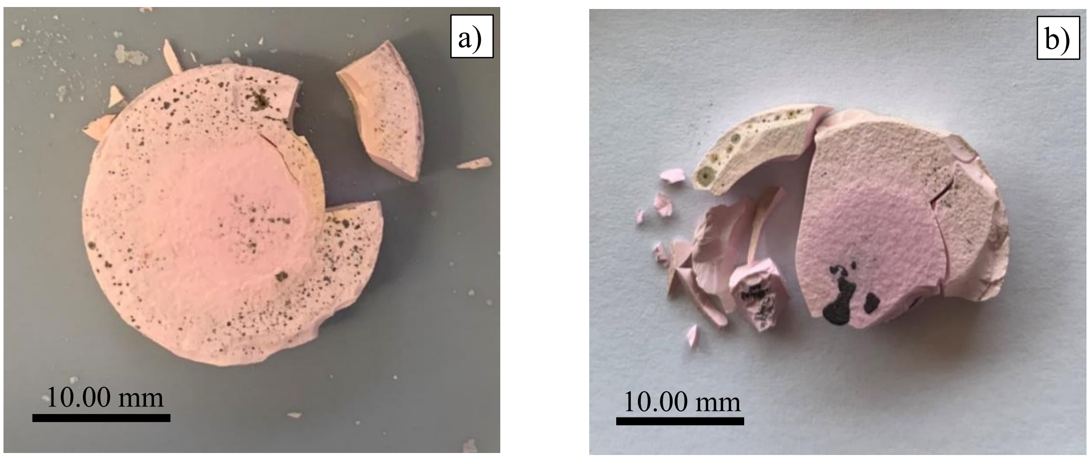

Figure 3.11: HERO powder sintered with RHEA substrate after TGA exposure of 1150°C for 5.5 hours in 1% O_2 in Ar. (a) displays Alloy 2-8, and (b) displays Alloy 1-3.

Figure 3.11 displays the coated alloys after 1150°C exposure in 1% O_2 in Ar for 5.5 hours in the TGA machine. The HERO coating on Alloy 2-8 had one large fragment crack and break off while under high temperature conditions, exposing about 5 – 10 mm of the side of the button of the alloy to the surrounding environment. Due to the issues highlighted above, there aren't reliable conclusions that can be drawn about the HERO coating cracking at these conditions, as it cannot be determined if the cracks and fragments seen in Figure 3.11 (b) were formed as a result of high temperature exposure or due to the sample falling through the tube.

The majority of cracked HERO fragments encompassing Alloy 1-3 fell to the bottom of the TGA tube and were not recovered.

3.4 XRD Analysis

Samples of Alloys 1-3 and 2-8 were analyzed with X-ray diffraction (XRD) techniques to characterize the oxide layers that formed during high temperature exposure in TGA studies. Alloy 2-8 was found to form TiO_2, $TiNb_2O_7$, and $Ti_2Nb_{10}O_{29}$. These results can be seen in Figure 3.12 where the number of counts versus diffraction angle are plotted.

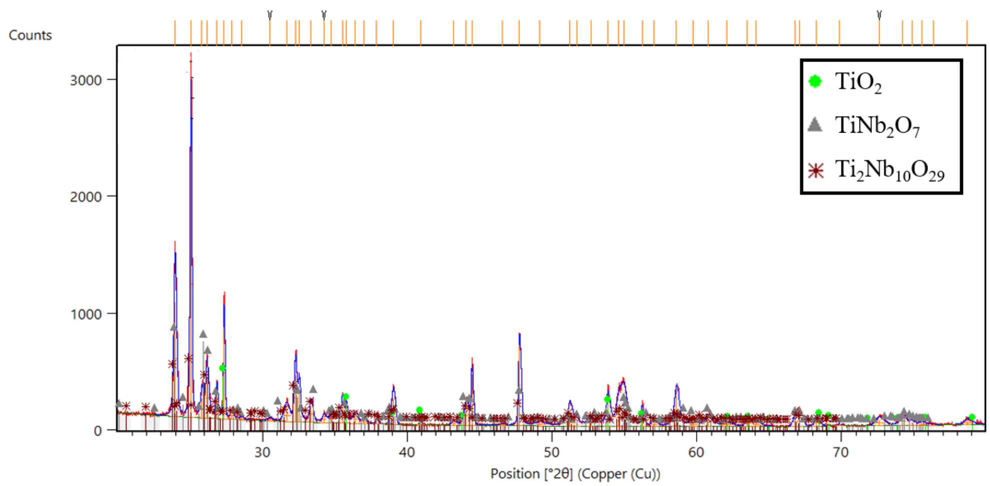

Figure 3.12: XRD analysis of Alloy 2-8 after undergoing TGA exposure of 1150°C for 5.5 hours in 1% O_2 in Ar.

Alloy 1-3 was found to form the complex oxides $TiNb_2O_7$ and $Ti_2Nb_{10}O_{29}$, which are identical to those formed in Alloy 2-8, in addition to the titanium oxide Ti_3O_5. These results can be seen in the intensity versus diffraction angle plot shown in Figure 3.13.

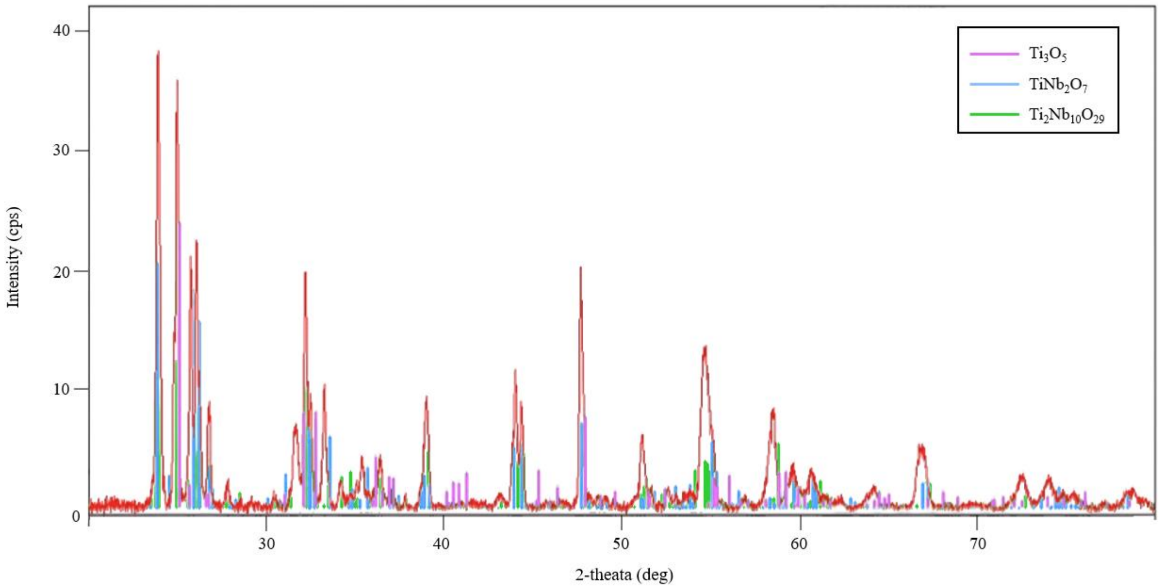

Figure 3.13: XRD analysis of Alloy 1-3 after undergoing TGA exposure of 1150°C for 5.5 hours in 1% O_2 in Ar.

Chapter 4. Conclusions & Future Work

4.1 Conclusions

The following conclusions can be drawn regarding Alloys 1-3 and 2-8, as well as their compatibility with a HERO coating, as a result of the studies described in this Thesis:

- Alloy 2-8 has large and small submicron secondary phase particles, whereas Alloy 1-3 only contains small submicron particles.
- TGA results show that both Alloys 2-8 and 1-3 demonstrate parabolic diffusion rate of oxidation; however, Alloy 2-8 has a smaller, less damaging mass gain.
- XRD results suggest that both Alloys 2-8 and 1-3 form nearly identical oxide layers during high temperature exposure.
- Dilatometry results support that Alloys 2-8 and 1-3 have similar coefficients of linear expansion, but larger CTEs than the HERO coating.
- HERO coated alloys tend to crack and fragment under high temperatures.

4.2 Future Work

Future work could entail:

- Exposures of coated and un-coated samples at 1150°C in 1% O_2 in Ar with time intervals of 1, 5, 10, and 20 hours

- Further analysis of the oxide layers formed at the RHEA surface and the depth of oxygen penetration into the substrate

Bibliography

[1] J.-W. Yeh, Recent Progress in High Entropy Alloys, Ann. Chim. Sci. Mat. 31 (2006) 633-648.

[2] D.-B. Miracle, A Critical Review of High Entropy Alloys and Related Concepts, Acta Materialia 122 (2017) 448-511.

[3] M.-H. Tsai, Physical Properties of High Entropy Alloys, Entropy 15 (2013) 5338-5345.

[4] T.-M. Butler, High Entropy Alloys: Oxidation, Elsevier (2020).

[5] S. Sheikh, Alloying Effect on the Oxidation Behavior of a Ductile AlCrNbTaTi Refractory High-Entropy Alloy, Materials Today Advances 7 (2020) 100104.

[6] B. Opila, High Entropy Rare-Earth Oxide (HERO) Thermal Environmental Barrier Coatings for Refractory Metal Alloys (2023), TMS, San Diego, CA.

[7] Kristyn Ardrey (2023). Thermochemical Degradation of Rare Earth-Based Environmental Barrier Coatings [Doctoral Dissertation, The University of Virginia].

[8] J. Daw, Joy Rempe, et. al. Variability of Pushrod Dilatometry Techniques for High Temperature In-Pile Measurements, 2008.

Appendix A. EDS Images of Alloy 2-8

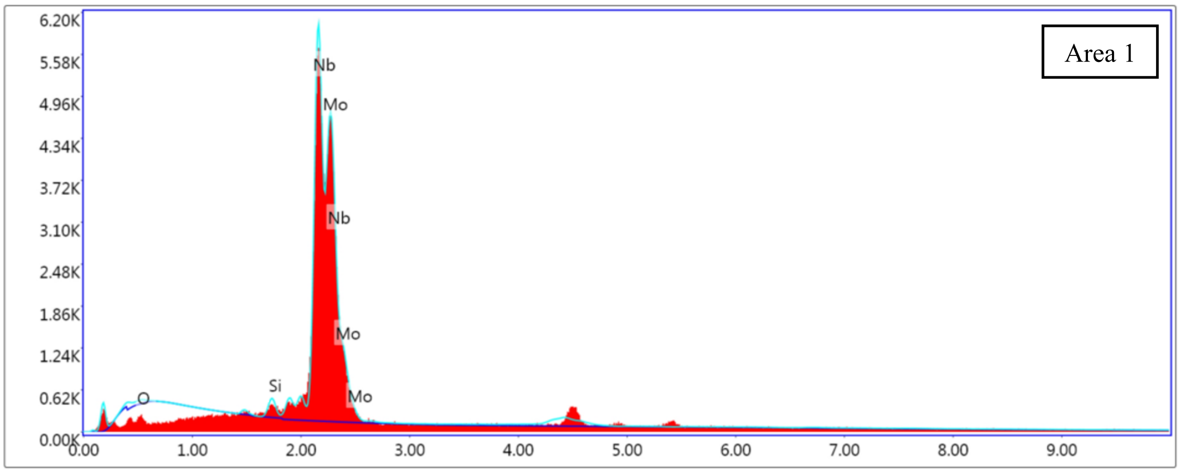

Figure A.1: EDS spectra of the lighter grey portion of the bulk material of Alloy 2-8, labeled as Area 1 in Figure 3.3.

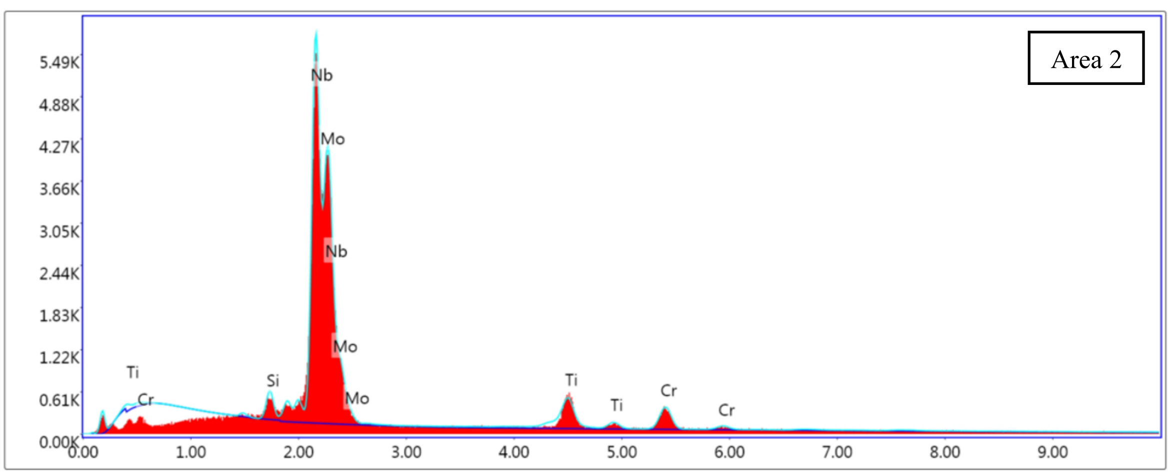

Figure A.2 EDS spectra of the lighter grey portion of the bulk material of Alloy 2-8, labeled as Area 2 in Figure 3.3.

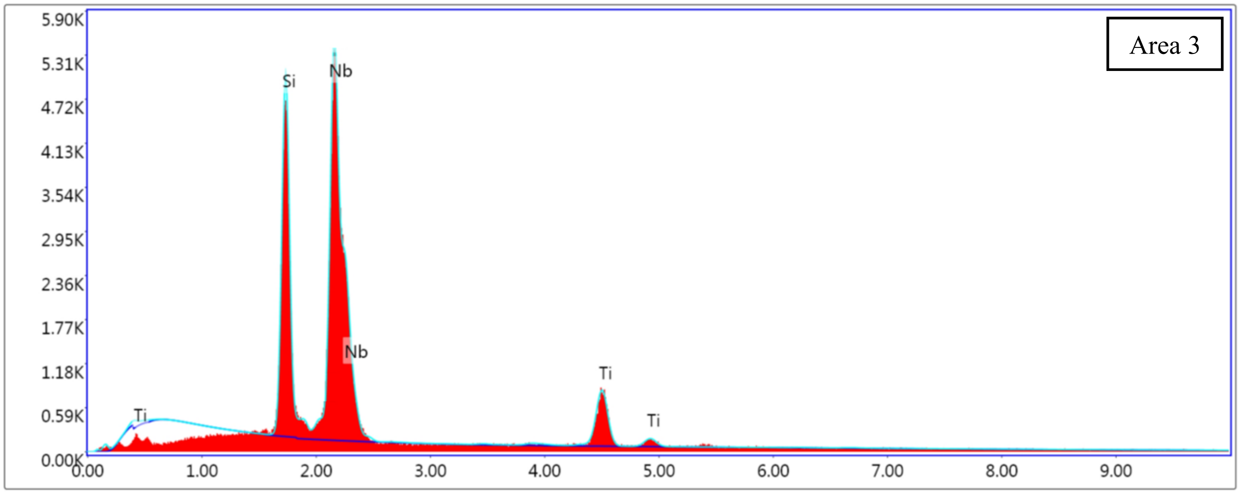

Figure A.3: EDS spectra of the darker grey secondary phase portion of Alloy 2-8, labeled as Area 3 in Figure 3.3.

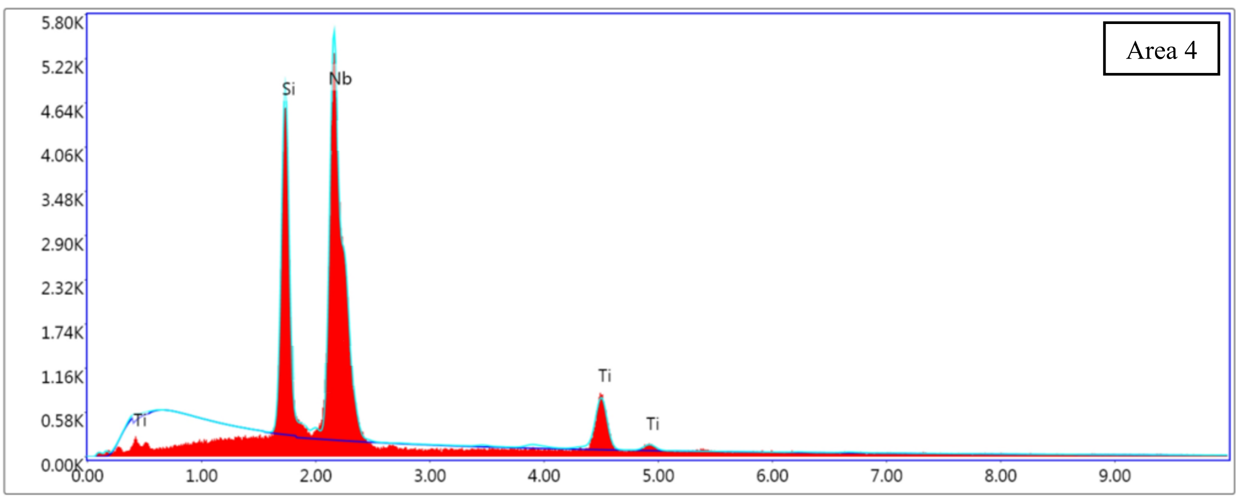

Figure A.4: EDS spectra of the darker grey secondary phase portion of Alloy 2-8, labeled as Area 4 in Figure 3.3.

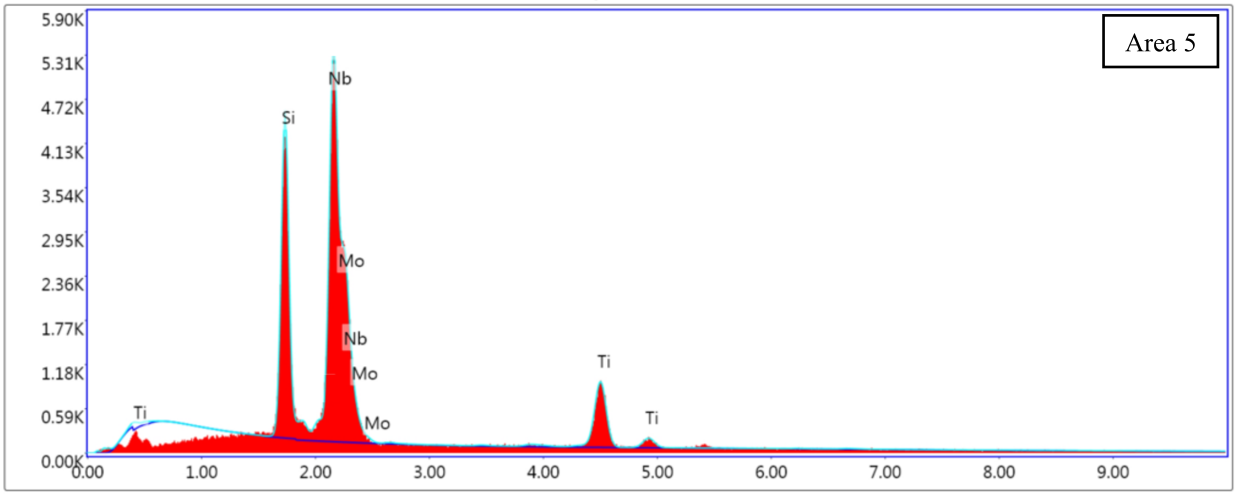

Figure A.5: EDS spectra of the darker grey secondary phase portion of Alloy 2-8, labeled as Area 5 in Figure 3.3.

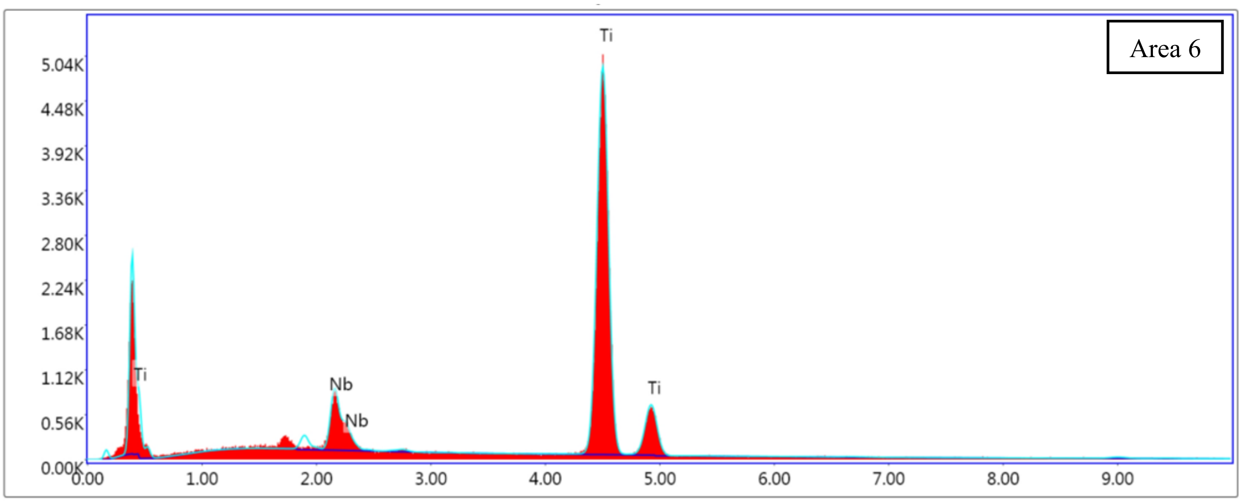

Figure A.6: EDS spectra of the black, submicron secondary phase particles in Alloy 2-8, labeled as Area 6 in Figure 3.3.

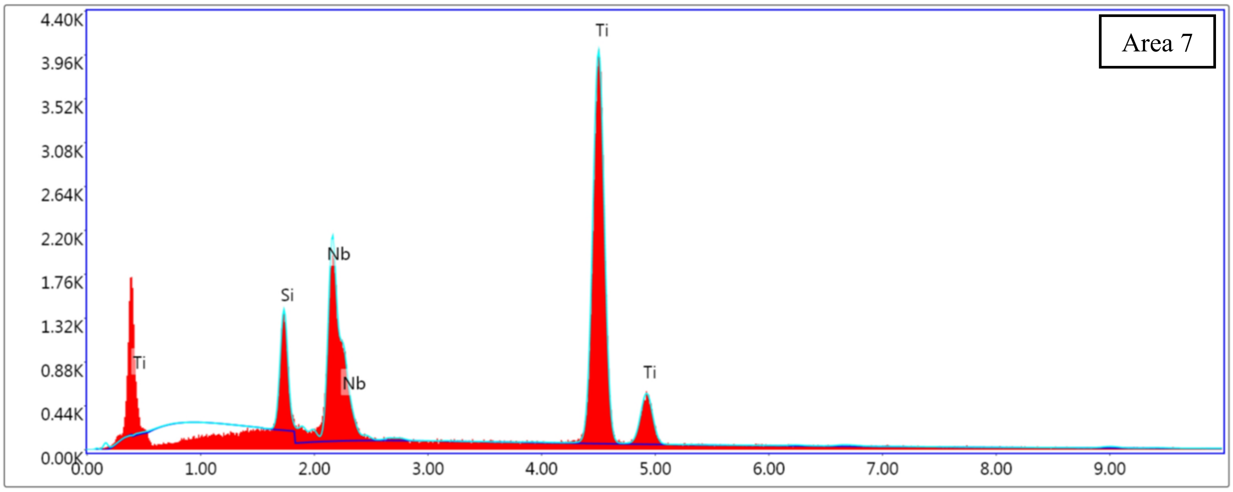

Figure A.7: EDS spectra of the black, submicron secondary phase particles in Alloy 2-8, labeled as Area 7 in Figure 3.3.